Near-Capacity Turbo Trellis Coded Modulation Design Based on EXIT Charts and Union Bounds

Soon Xin Ng, *Member, IEEE*, Osamah Rashed Alamri, *Student Member, IEEE*, Yonghui Li, *Member, IEEE*, Jörg Kliewer, *Senior Member, IEEE*, and Lajos Hanzo, *Fellow, IEEE*

***Abstract*— Bandwidth efficient parallel-concatenated Turbo Trellis Coded Modulation (TTCM) schemes were designed for communicating over uncorrelated Rayleigh fading channels. A symbol-based union bound was derived for analysing the error floor of the proposed TTCM schemes. A pair of In-phase (I) and Quadrature-phase (Q) interleavers were employed for interleaving the I and Q components of the TTCM coded symbols, in order to attain an increased diversity gain. The decoding convergence of the IQ-TTCM schemes was analysed using symbol-based EXtrinsic Information Transfer (EXIT) charts. The best TTCM component codes were selected with the aid of both the symbol-based union bound and non-binary EXIT charts, for designing capacity-approaching IQ-TTCM schemes in the context of 8PSK, 16QAM, 32QAM and 64QAM modulation schemes.**

***Index Terms*— Decoding convergence, distance spectrum, code design, EXIT charts, Turbo Trellis Coded Modulation, union bound.**

I. Introduction

Trellis Coded Modulation (TCM) [1] was originally proposed for transmission over Additive White Gaussian Noise (AWGN) channels, but later it was further developed for applications in mobile communications [2], [3], since it accommodates all the parity bits by expanding the signal constellation, rather than increasing the bandwidth requirement. Turbo Trellis Coded Modulation (TTCM) [4] is a more recent joint coding and modulation scheme that has a structure similar to that of the family of power-efficient binary turbo codes [5], but employs two identical parallel concatenated TCM schemes as component codes. A symbol-based turbo interleaver is used between the two TCM encoders and the encoded symbols of each component code are punctured alternatively for the sake of achieving a higher bandwidth efficiency as detailed in [4], [6]. The design of the TTCM scheme outlined in [4] was based on the search for the best component TCM codes using the so-called 'punctured' minimal distance criterion, where the constituent TCM codes having the maximal 'punctured' minimal distance were sought. However, the TTCM schemes designed for AWGN channels in [4] would exhibit a high error floor, when communicating over Rayleigh fading channels, if any information bits are unprotected by the constituent component codes [7]. Hence, a different TTCM design is needed, when communicating over Rayleigh fading channels.

It was shown in [2] that the maximisation of the minimum Hamming distance measured in terms of the number of different symbols between any two transmitted symbol sequences is the key design criterion for TCM schemes contrived for uncorrelated Rayleigh fading channels, where the fading coefficients change independently from one symbol to another. More specifically, Bit-Interleaved Coded Modulation (BICM) [8] employing bit-based interleavers was designed for increasing the achievable diversity order to the binary Hamming distance of a code for transmission over uncorrelated Rayleigh fading channels. A parallel-concatenated Turbo BICM scheme was designed in [9] and was analysed in [10] when communicating over Rayleigh fading channels, where a lower error floor is attained as a benefit of having a higher minimum Hamming distance. However, bit-interleaved turbo coding schemes have a poorer decoding convergence [11] compared to their symbol-interleaved counterparts due to the associated information loss, when invoking a bit-to-symbol probability conversion during each decoding iteration [12]. Hence, it is desirable to reduce the error floor without using a bit-based interleaver in order to retain the good convergence properties of symbol-interleaved turbo coding schemes.

More specifically, apart from using bit interleavers, the diversity order of a code can be increased with the aid of spatial diversity, frequency diversity and signal space diversity [13]. More explicitly, signal space diversity is obtained by employing two independent channel interleavers for separately interleaving the In-phase (I) and Quadrature-phase (Q) components of the complex-valued encoded signals, combined with constellation rotation. A TCM scheme designed with signal space diversity was proposed in [14]. On the other hand, it was shown in [15] that a diversity gain may also be attained using IQ interleaving alone – i.e. without constellation rotation – in the context of TCM and TTCM schemes. The diversity associated with IQ interleaving alone was referred to as IQ-diversity [15], where the error floor of the IQ-diversity assisted TTCM (IQ-TTCM) schemes was lower than that of conventional TTCM schemes [15]. Hence, we will design new TTCM schemes employing symbol-based turbo interleavers for attaining an early decoding convergence as well as separate I and Q channel interleavers for achieving a low error floor.

S. X. Ng, O. R. Alamri and L. Hanzo are with the School of Electronics and Computer Science, University of Southampton, SO17 1BJ, United Kingdom. Email: {sxn,ora02r,lh}@ecs.soton.ac.uk.

Y. Li is with the School of Electrical & Information Engineering, University of Sydney, Sydney, NSW, 2006, Australia. Email: lyh@ee.usyd.edu.au

J. Kliewer is with the Klipsch School of Electrical and Computer Engineering, New Mexico State University, Las Cruces, NM 88003, U.S.A. E-mail: jkliewer@nmsu.edu

The financial support of the European Union under the auspices of the Newcom and Phoenix projects, as well as that of the EPSRC UK, the Ministry of Higher Education of Saudi Arabia and the German Research Foundation (DFG) is gratefully acknowledged.

Note that turbo codes exhibit low a Bit Error Rate (BER) in the low to medium Signal to Noise Ratio (SNR) region due to their early decoding convergence. The asymptotic BER performance of a code at high SNR is mainly dominated by its minimum distance. However, the overall BER performance of a code is influenced not only by the minimum distance, but by several distance spectral components, in particular in the medium SNR region [16]–[18]. Hence, the accurate Distance Spectrum [19] analysis has to consider several distance spectral lines, when designing a turbo-style code. Note further that the overall BER performance of a code is determined by both the effective Hamming distance and the effective product distance, when communicating over uncorrelated Rayleigh fading channels [2]. Hence, a two-Dimensional (2D) distance spectrum constituted by both the Hamming distance and product distance has to be evaluated [20]. Recently, a TTCM scheme employing bit-based turbo interleavers was proposed and analysed in [20], where the corresponding union bound of the BER was derived based on the 2D distance spectrum. However, the convergence of the bit-interleaved TTCM of [20] was again inferior compared to the symbol-interleaved TTCM design, despite having a lower error floor. We will derive the BER union bound for TTCM schemes employing symbol-based turbo interleavers in order to analyse their error floor performance.

EXtrinsic Information Transfer (EXIT) charts constitute useful tools, when analysing the convergence properties of iterative decoding schemes. They have been invoked for analysing both concatenated binary coding schemes [21] and non-binary coding schemes [22], [23]. As a result, near-capacity codes have been successfully designed by applying an EXIT chart based technique in [24], [25]. *The novel contribution of this paper is that we will employ the low-complexity symbol-based EXIT charts proposed in [23] and the corresponding BER union bound of the TTCM schemes in order to design new, near-capacity symbol-interleaved TTCM schemes.* More specifically, new Generator Polynomials (GPs) are sought for the TCM component codes, based on their decoding convergence and on the error floor performance of the TTCM decoder, rather than on the 'punctured' minimal distance criterion of the TCM component codes defined in [4]. Our prime design criterion is to find a constituent TCM code, where the corresponding EXIT charts exhibit an open tunnel at the lowest possible SNR value, as well as having an acceptable error floor as estimated by the truncated symbol-based union bound.

The rest of the paper is organised as follows. The system model is described in Section II. The novel symbol-based union bound of the BER of the TCM and TTCM schemes are derived based on the 2D distance spectrum in Section III. An overview of the symbol-based EXIT charts is given in Section IV. Our novel constituent code search algorithm is detailed in Section V and the resultant findings are presented and discussed in Section VI. Finally, our conclusions are offered in Section VII.

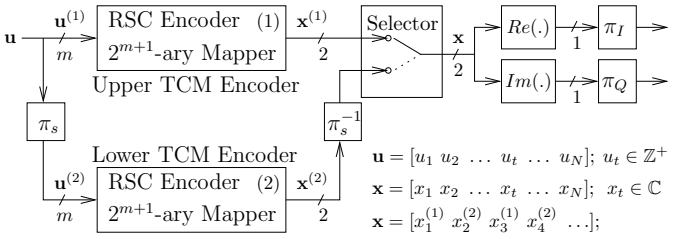

Fig. 1. Schematic of an IQ-TTCM encoder.

II. System Model

In this paper, we consider only two-dimensional TCM and TTCM schemes, where the code rate is given by $R = m/(m+1)$, employing 2^{m+1}-ary PSK/QAM signal sets. Hence the effective throughput is m bit per modulated symbol. A TCM encoder consists of a Recursive Systematic Convolutional (RSC) encoder and a signal mapper. An IQ-interleaved TTCM encoder employing two TCM component schemes is shown in Fig. 1. The N-symbol uncoded and encoded symbol sequences are denoted as $\mathbf{u}$ and $\mathbf{x}$, respectively. The superscripts (1) and (2) are used for differentiating the uncoded and encoded sequences belonging to the upper and lower TCM encoders, respectively. The I and Q channel interleavers, namely π_I and π_Q, are used for independently interleaving the I and Q components of the complex-valued encoded symbol sequence $\mathbf{x}$.

Note that a TTCM scheme employs an Odd-Even Separation (OES) based symbol interleaver π_s as the turbo interleaver, where odd (even) indexed symbols are mapped to another odd (even) position after interleaving. An OES symbol deinterleaver π_s^{-1} is also used at the output of the lower TCM encoder. This ensures that after the alternative puncturing, which is performed by the 'Selector' block shown in Fig. 1, all even (odd) indexed symbols of the upper (lower) TCM component encoder are punctured [4]. Note that the information parts of each encoded symbol from the upper and lower TCM encoders before the 'Selector' block are identical. Hence, the information bits are transmitted exactly once. Let us denote the punctured encoded symbol as $x0_t^{(j)}$ for $j \in \{1, 2\}$, where the m information bits are retained, but the parity bit is set to zero. Hence, we may view the actual transmitted encoded symbol sequences from the upper and lower TCM encoders as:

$$\mathbf{x}^{(1)} = [x_1^{(1)}\ x0_2^{(1)}\ x_3^{(1)}\ x0_4^{(1)}\ x_5^{(1)}\ x0_6^{(1)}\ \ldots] \ , \tag{1}$$

and

$$\mathbf{x}^{(2)} = [x0_1^{(2)}\ x_2^{(2)}\ x0_3^{(2)}\ x_4^{(2)}\ x_5^{(2)}\ x0_6^{(2)}\ \ldots] \ , \tag{2}$$

respectively, while the TTCM encoded symbol sequence is:

$$\mathbf{x} = [x_1^{(1)}\ x_2^{(2)}\ x_3^{(1)}\ x_4^{(2)}\ x_5^{(1)}\ x_6^{(2)}\ \ldots] \ . \tag{3}$$

Note that for simplicity we do not differentiate the sequences before and after the turbo interleaver.

III. Symbol-based Union Bounds

Let us define the encoded symbol sequence and the erroneously detected symbol sequence of N symbol durations as

$\mathbf{x} = [x_1\ x_2\ \ldots\ x_t\ \ldots\ x_N]$ and $\hat{\mathbf{x}} = [\hat{x}_1\ \hat{x}_2\ \ldots\ \hat{x}_t\ \ldots\ \hat{x}_N]$, respectively. When communicating over uncorrelated Rayleigh fading channels, the Pair-Wise Error Probability (PWEP) of erroneously detecting the sequence $\hat{\mathbf{x}}$ instead of sequence $\mathbf{x}$ can be upper bounded by the following exact-polynomial bound [26, Eq. (35)]:

$$P_{\text{PWEP}}(\mathbf{x} \to \hat{\mathbf{x}}) \quad \leq \quad \binom{2\Delta_H - 1}{\Delta_H - 1} \left(\frac{E_s}{N_0}\right)^{-\Delta_H} (\Delta_P)^{-1} \quad (4)$$

which is tighter than the Chernoff bound of [2]. More explicitly, E_s/N_0 is the average channel SNR, Δ_H is referred to as the *effective Hamming distance*, which quantifies the diversity order of the code and Δ_P is termed as the *effective product distance*, which quantifies the coding advantage of a code. More specifically, the product distance of a TCM code is defined as the product of the non-zero squared Euclidean distances along the error path:

$$\Delta_P = \Delta_P(\mathbf{x}, \hat{\mathbf{x}}) = \prod_{t \in \eta} |x_t - \hat{x}_t|^2 \ , \quad (5)$$

where η represents the set of symbol indices t satisfying the condition of $x_t \neq \hat{x}_t$, for $1 \leq t \leq N$, while the number of elements in the set η is given by $\Delta_H = \Delta_H(\mathbf{x}, \hat{\mathbf{x}})$, which quantifies the number of erroneous symbol in the sequence $\hat{\mathbf{x}}$, when compared to the correct sequence $\mathbf{x}$.

For the parallel concatenated TTCM scheme, the 'punctured' encoded symbol sequences of the upper and lower TCM encoders, namely $\mathbf{x}^{(1)}$ and $\mathbf{x}^{(2)}$ of Eqs. (1) and (2), respectively, are transmitted at different time instants and hence they are independent of each other. Therefore, the product distance between the TTCM encoded symbol sequences $\mathbf{x}$ and $\hat{\mathbf{x}}$ is given by the product of the individual product distances of the upper and lower TCM-encoded symbol sequences as follows:

$$\Delta_P \quad = \quad \Delta_P^{(1)} \cdot \Delta_P^{(2)} \ , \quad (6)$$

where $\Delta_P^{(j)} = \Delta_P(\mathbf{x}^{(j)}, \hat{\mathbf{x}}^{(j)})$ for $j \in \{1, 2\}$. Furthermore, the resultant Hamming distance of TTCM is given by the sum of the Hamming distances of the upper and lower TCM codes as:

$$\Delta_H \quad = \quad \Delta_H^{(1)} + \Delta_H^{(2)} \ , \quad (7)$$

where $\Delta_H^{(j)} = \Delta_H(\mathbf{x}^{(j)}, \hat{\mathbf{x}}^{(j)})$ for $j \in \{1, 2\}$.

The union bound of the average BER of a coding scheme communicating over uncorrelated Rayleigh fading channels can be derived based on [27, p. 125] as:

$$P_b \quad \leq \quad \frac{1}{m} \sum_{\Delta_P} \sum_{\Delta_H} B_{\Delta_P, \Delta_H} P_{\text{PWEP}} \ , \quad (8)$$

where m is the number of information bits per symbol and B_{Δ_P, Δ_H} is the 2D distance spectrum of the code, given by:

$$B_{\Delta_P, \Delta_H} \quad = \quad \sum_{w} \frac{w}{N} \cdot A_{w, \Delta_P, \Delta_H} \ , \quad (9)$$

where w is the information weight denoting the number of erroneous information bits in an encoded N-symbol sequence. Furthermore, $A_{w, \Delta_P, \Delta_H}$ is the three-dimensional Weight Enumerating Function (WEF), quantifying the average number of sequence error events having an information weight of w, a product distance of Δ_P and a Hamming distance of Δ_H.

A. TCM Distance Spectrum

Let us derive the WEF $A_{w, \Delta_P, \Delta_H}$ for a TCM scheme having a block length of N encoded symbols and let the total number of trellis states be M. We can define the State Input-Redundancy WEF (SIRWEF) for a block of N TCM-encoded symbols as:

$$\mathbf{A}(N, S, W, Y, Z) \quad = \quad \sum_{w} \sum_{\Delta_P} \sum_{\Delta_H} A_{N, S, w, \Delta_P, \Delta_H} \cdot W^w Y^{\Delta_P} Z^{\Delta_H} \ , \quad (10)$$

where $A_{N, S, w, \Delta_P, \Delta_H}$ is the number of paths in the trellis entering state S at symbol index N, which have an information weight of w, a product distance of Δ_P and a Hamming distance of Δ_H. The notations W, Y and Z represent dummy variables. For each symbol index t, the term $A_{t, S, w, \Delta_P, \Delta_H}$ can be calculated recursively as follows:

$$A_{t, S, w, \Delta_P, \Delta_H} = \sum_{S', S: u_t} A_{t-1, S', w', \Delta'_P, \Delta'_H} \ , \ (1 \leq t \leq N) \quad (11)$$

where u_t represents the specific input symbol that triggers the transition from state S' at index $(t-1)$ to state S at index t, while the terms w, Δ_P and Δ_H can be formulated as:

$$w \quad = \quad w' + i(S', S) \ , \quad (12)$$

$$\Delta_P \quad = \quad \begin{cases} \Delta'_P \cdot \Theta(S', S) \ , & \text{if } \Theta(S', S) > 0 \\ \Delta'_P \ , & \text{else} \end{cases} \quad (13)$$

$$\Delta_H \quad = \quad \Delta'_H + \Phi(S', S) \ , \quad (14)$$

where w', Δ'_P and Δ'_H are the information weight, the product distance and the Hamming distance, respectively, of the trellis paths entering state S' at index $(t-1)$. Furthermore, $i(S', S)$ is the information weight of symbol u_t that triggers the transition from state S' to S, while $\Theta(S', S) = |x_t - \hat{x}_t|^2$ and $\Phi(S', S) \in \{0, 1\}$ are the squared Euclidean distance and Hamming distance between the encoded symbols $\hat{x}_t$ and x_t, where $\hat{x}_t$ is the encoded symbol corresponding to the trellis branch in the transition from state S' to S and x_t is the actual transmitted encoded symbol at index t. Let the encoding process commence from state 0 at index 0 and terminate at any of the M possible states at index N. Then the WEF used in Eq. (9) is given by:

$$A_{w, \Delta_P, \Delta_H} = \sum_{S} A_{N, S, w, \Delta_P, \Delta_H} \ . \quad (15)$$

Note that for linear codes [28] or for the *strong-sense* regular TCM schemes defined in [29], the distance profile of the code is independent of which particular encoded symbol sequence is considered to be the correct one. Hence, for the sake of simplicity, we can assume that the all-zero encoded symbol sequence is transmitted, where the union bound of a strong-sense regular TCM scheme can be computed based on Eq (8) using both the PWEP of Eq (4) and the 2D distance spectrum of Eq (9). By contrast, for TCM schemes which are not strong-sense regular as defined in [29], we have to consider all possible correct sequences in order to generate the distance spectrum, and hence a more sophisticated algorithm such as that proposed in [29] is needed. However, the objective of this paper is not to find the exact union bound of the

general TCM or TTCM schemes, but to use the 'approximate' union bound to design near-capacity TTCM schemes. Hence, we will only consider the all-zero encoded symbol sequence as the correct sequence, when computing the union bound. We found that since most TCM and TTCM schemes are not strong-sense regular, applying tailing symbols for having a trellis terminated at state 0 at index N provides a marginal performance improvement compared to having non-terminated trellis, when communicating over uncorrelated Rayleigh fading channels. Furthermore, the union bound computed based on the exact-polynomial bound of Eq. (4) using the all-zero encoded sequence as the correct sequence turns out to be a very tight bound when approximating the BER performance of various TCM schemes employing 8PSK, 16QAM and 32QAM, as we will demonstrate in Section VI.

B. TTCM Distance Spectrum

Let us now derive the WEF A_{w,Δ_P,Δ_H} introduced in Eq. (9) for a TTCM scheme. Since a TTCM scheme employs two TCM constituent codes, where the parity bits of the upper and lower TCM encoded symbols are punctured at the even and odd symbol indices, respectively, we have to compute two separate distance spectra for the two punctured TCM component codes. Let us denote the SIRWEF of the upper and lower TCM component codes by $\mathbf{A}^{(1)}(N,S,W,Y,Z)$ and $\mathbf{A}^{(2)}(N,S,W,Y,Z)$, respectively. Note that all the punctured parity bits are considered to have a value of '0' when computing the two SIRWEF terms. We also assume that no termination symbols are used since their performance benefits were found to be modest. Hence both the trellises may be terminated in any of the M possible trellis states. Then we may compute the WEF of the TTCM scheme from the WEF of the two punctured TCM component codes as:

$$A_{w,\Delta_P,\Delta_H} = A^{(1)}_{w,\Delta_P^{(1)},\Delta_H^{(1)}} \cdot A^{(2)}_{w,\Delta_P^{(2)},\Delta_H^{(2)}} \cdot P_{oe}^{N,w} \ , \qquad (16)$$

where $\Delta_P = \Delta_P(\mathbf{x},\hat{\mathbf{x}})$ and $\Delta_H = \Delta_H(\mathbf{x},\hat{\mathbf{x}})$ are defined in Eqs (6) and (7), respectively. The term $P_{oe}^{N,w}$ in Eq (16) denotes the probability of occurrence for all the associated error events having w information bit errors, when employing an OES symbol interleaver having a length of N symbols. Note that this term equals $1/\binom{N}{w}$, when a bit-based random interleaver of length N scrambling 1-bit symbols is employed as the turbo interleaver, as in [30]. The value of $P_{oe}^{N,w}$ is computed based on the uniform OES symbol interleaver concept, which is developed by extending the uniform bit interleaver proposed in [30]. More specifically, an OES symbol interleaver may be partitioned into two symbol interleavers, where the number of bits per symbol equals the number of information bits per symbol, namely m, since we are only concerned with the information bit errors as in [30]. The uniform OES symbol interleaver may be defined as in Definition 1.

Definition 1: A uniform OES symbol interleaver of length N symbols is a probabilistic device, which maps a given input sequence of length N symbols having an information weight of w bits into all possible combinations in the odd and even partitions of the interleaver, with equal probability of $P_{oe}^{N,w}$ given by:

$$P_{oe}^{N,w} = \sum_{\substack{w_o=0 \\ (w_o+w_e=w)}}^{w_o=w} P_m^{\lceil N/2\rceil,w_o} \cdot P_m^{\lfloor N/2\rfloor,w_e} \ , \qquad (17)$$

where w_o and w_e are the number of bit errors in the odd and even partitions of the OES symbol interleaver and the term $P_m^{L,y}$ denotes the probability of occurrence for the error event having y information bit errors when employing a uniform symbol interleaver of length L symbols, where $L \in \{\lceil N/2\rceil, \lfloor N/2\rfloor\}$ and m is the number of bits per symbol. More explicitly, we have:

$$P_m^{L,y} = \frac{1}{\sum_{z\in\chi(y,m)}\binom{L}{z}} \ , \qquad (18)$$

where the set $\chi(y,m)$ consists of all possible combinations of the z number of symbol errors for a given number of bit errors y in a sequence of L symbols. Explicitly, this set is given by:

$$\chi(y,m) = \left\{ z := \sum_{b=1}^{m} z_b; \quad \text{for} \sum_{b=1}^{m} b\cdot z_b = y \right\} \ , \qquad (19)$$

where the number of symbol errors each having b bit errors is z_b.

The computation of the set $\chi(y,m)$ is given in the Appendix.

IV. Symbol-based EXIT Charts

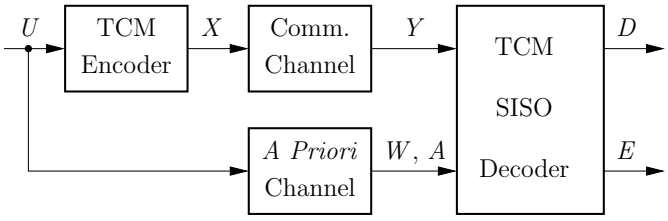

Fig. 2. Decoding model for a parallel concatenated TTCM scheme.

The decoding model for one of the two constituent TCM codes of the parallel concatenated TTCM scheme can be represented by Fig. 2, where the information symbol sequence U is encoded by the constituent TCM encoder, generating the encoded symbol sequence X. The sequence X is transmitted over the communications channel and the received symbol sequence is denoted by Y. The *a priori* channel models the generation of the extrinsic information by the other TCM decoder and the sequence W can be thought of as the hypothetical channel-impaired – i.e. error-prone – sequence, when the information sequence U was transmitted over the *a priori* channel. Furthermore, the *a priori* symbol probabilities A of the TCM-encoded symbols fed to the SISO decoder of Fig. 2 represent the *extrinsic* symbol probabilities that can be extracted from the output of the other TCM decoder. Based on both Y and A, the SISO decoder computes both the *a posteriori* symbol probabilities D and the *extrinsic* symbol probabilities E.

We note that the *extrinsic* and the systematic information associated with each *a posteriori* TTCM symbol probability at the output of a constituent TCM decoder cannot be separated,

since the systematic and parity bits of a TTCM encoded symbol are transmitted together in a modulated symbol over the communication channels [4], [6]. However, we have to extract the *extrinsic* information from the *a posteriori* symbol probability in order to generate the corresponding symbol-based EXIT chart [31]. Hence, the assumption that the *extrinsic* and systematic information are independent of each other is needed [31], so that the *extrinsic* information may be extracted from the *a posteriori* symbol probability. Nonetheless, despite the limited validity of the above-mentioned independence, we will show in Section VI that accurate code design is still possible with the aid of the resultant EXIT charts.

An efficient method devised for generating symbol-based EXIT charts from symbol-based *a posteriori* probabilities (APPs) was proposed in [23]. This technique is based on the fact that the symbol-based APPs generated at the output of a SISO decoder represent sufficient statistics for all observations (channel and *a priori* information) at its input. More specifically, the average extrinsic information $I_E(u)$ at the output of the APPs decoder can be computed as [23]:

$$I_E(u) = \log_2(\mathcal{M}) - \frac{1}{N}\sum_{k=1}^{N} \mathrm{E}\left[\sum_{i=1}^{\mathcal{M}} e(u_k^{(i)}) \log_2(e(u_k^{(i)}))\right] \tag{20}$$

where N is the number of information symbols in the decoding block, $\mathcal{M} = 2^m$ is the cardinality of the m-bit information symbol, $u_k^{(i)}$ is the hypothetically transmitted information symbol at time instant k for $i \in \{1, 2, \ldots, \mathcal{M}\}$, $e([.])$ is the extrinsic probability of symbol $[.]$ and the expectation can be approximated by simple time-averaging of the extrinsic probabilities of the information symbol. As an advantage, the symbol-based extrinsic mutual information can be computed using Eq. (20) at a considerably lower complexity compared to the conventional histogram-based approach.

V. Constituent Code Search

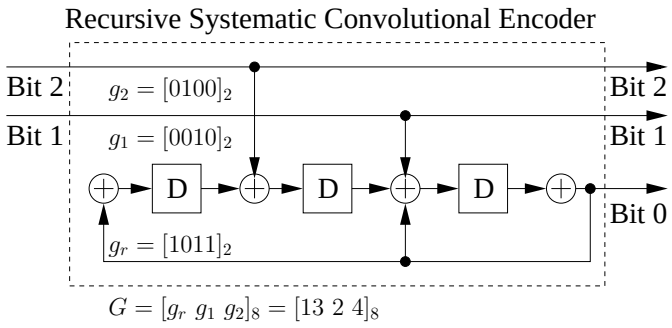

Fig. 3. TCM constituent component code.

Let us first consider the RSC encoder structure of a constituent TCM component code seen in Fig. 3, which depicts the RSC encoder used by the constituent TCM component code of an 8-state 8PSK-based TTCM scheme. The number of information bits per symbol is $m = 2$ and there is only one parity bit in each TCM encoded symbol. Hence, the code rate is $R = m/(m+1)$. The connections shown in Fig. 3 between the information bits and the modulo-2 adders are given by the GPs. The feed-forward GPs are denoted as g_i for $i \in \{1, 2 \ldots, m\}$, while the feed-back GP is denoted as g_r. As shown in Fig. 3, there are 4 possible connection points, when there are three shift register stages, each denoted by D. The four binary digits seen in the GPs indicate the presence or absence of connections. For example, the GP corresponding to the first information bit, namely Bit 1, is given by $g_1 = [0010]_2$, which indicates that Bit 1 is connected only to the modulo-2 adders that is third from the left. Note that we follow one of the rules provided in [1], where the right-most connection point is connected to the parity bit only, so that all the paths diverging from a common trellis state are associated with codewords having the same parity bit, but at least one different systematic bit [1]. The code GP is expressed in octal format as $G = [g_r\ g_1\ g_2]_8 = [13\ 2\ 4]_8$.

The constituent TCM code search used for finding meritorious TTCM schemes was originally based on the 'punctured' minimal distance criterion [4]. However, we found that a constituent code having the 'punctured' maximal minimal distance guaranteed the highest coding gain only during the first turbo iteration, but it was unable to always guarantee a decoding convergence at the lowest possible SNR value. By contrast, the EXIT chart characteristics had the ability to predict decoding convergence, where decoding convergence is indicated by having an open tunnel between the two EXIT chart curves [21]. Therefore, the 'punctured' maximal minimal distance is no longer the prime criterion, when designing capacity-approaching TTCM schemes. Instead, the prime design criterion is to find a constituent TCM code, where the corresponding EXIT charts exhibit an open tunnel at the lowest possible SNR value, as well as an acceptable error floor as estimated by the symbol-based union bound outlined in Section III.

Since maximising the minimal distance is no longer the main design objective, we can predefine the GP connections of the information bits and then only search for the best GP creating the parity bit. On one hand, using different GPs for the information bits may result in a different optimal parity-bit GP. On the other hand, we found that having a single connection for each of the information bits to a single distinct modulo-2 adder, as in Fig. 3, and then searching for the best parity-bit GP, namely g_r, had the potential of providing us with constituent TCM component codes creating near-capacity TTCM schemes. When the number of modulo-2 connections for each of the information bits to the shift registers is set to one, the correlation between the information bits and the parity bit is minimised. Hence the potential EXIT chart and decoding-trajectory mismatch may be reduced. Furthermore, when the GPs of the m number of systematic information bits are predefined, the search space is reduced from $2^{m\nu}$ to 2^{ν}, where ν is the number of shift register stages. Since each information bit may only have a distinct connection to a single modulo-2 adder, the minimum number of shift register stages required equals the number of information bits, i.e. we have $\nu = m$.

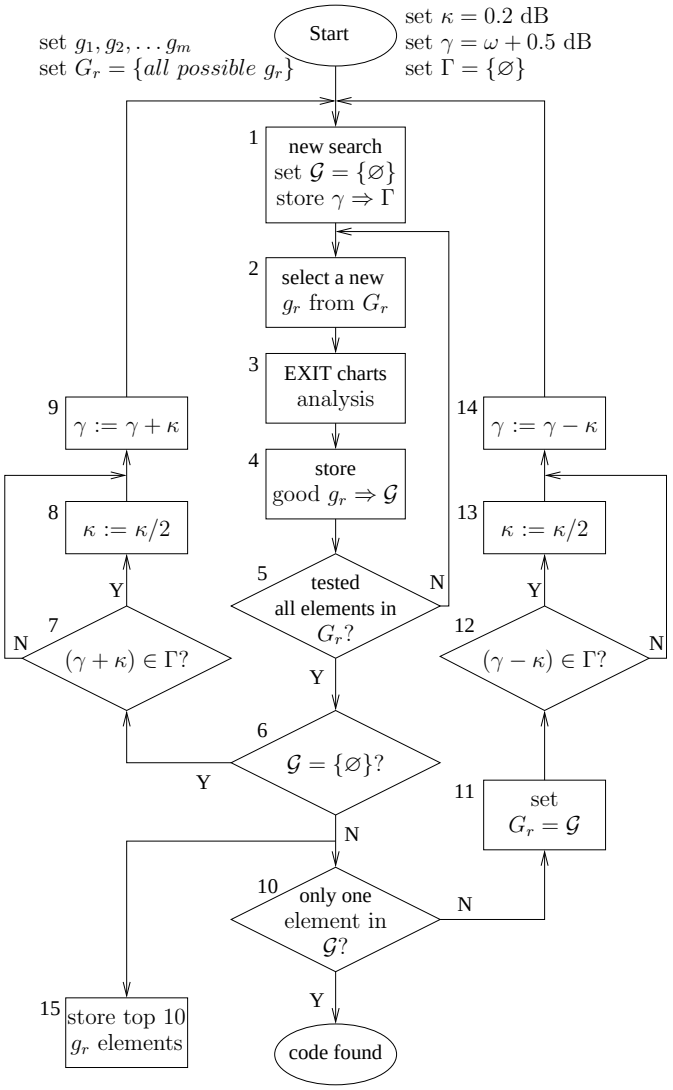

Fig. 4. Code search algorithm.

A. Code Search Algorithm

We derive a code-search algorithm for finding the TCM constituent codes using the symbol-based EXIT charts of [23], which is summarised in the flow chart shown in Fig. 4. The algorithm commences by initialising five parameters. Firstly, the GPs of the m information bits are initialised. Secondly, the feedback polynomial set G_r was constructed by storing all the 2^ν possible parity bit polynomials g_r. Thirdly, a step size of $\kappa = 0.2$ dB was set. Fourthly, the initial value for the average SNR per information bit, namely E_b/N_0 was set to $\gamma = \omega + 0.5$ dB, where ω is the corresponding E_b/N_0 value at a channel capacity of m bit/symbol, which is equivalent to the overall code rate. Finally, the set Γ was introduced for storing the E_b/N_0 values, which was initialised as a null set. Then the parity bit GP search begins by initialising the 'good code' set $\mathcal{G}$ to a null set. Then the current E_b/N_0 value, namely γ, was assigned to the set Γ.

The GP search procedure consisting of blocks 2, 3 and 4 constitutes the core of the algorithm, where the EXIT chart of each tentatively tested GP invoking a new polynomial g_r from the full set G_r was computed in Block 3. If there is an open tunnel in its EXIT chart, then the resultant TCM code is considered a meritorious code and the corresponding g_r value is stored in the 'good code' set $\mathcal{G}$ at Block 4. The search for near-capacity TCM codes continues, until all elements in the full parity-polynomial set G_r are tested. If none of the polynomials g_r in the set G_r is free from an EXIT-chart crossover, i.e. we have $\mathcal{G} = \{\varnothing\}$, the algorithm proceeds to Block 7. However, if there are more than one elements in the set $\mathcal{G}$, we reinitialise the set G_r using the newly found 'good code' set $\mathcal{G}$ and proceed to Block 12. Note that we do not have to search for all possible parity bit polynomials g_r again, when visiting the main procedure (blocks 2, 3 and 4) this time, since G_r consists of parity bit polynomials found during the previous search, which are capable of approaching the achievable capacity. When there is only one element in the set $\mathcal{G}$ at Block 10, we have found the best TCM component code and the search is concluded, where the estimated decoding convergence threshold is given by the corresponding E_b/N_0 value, namely γ.

The operations represented by blocks 12, 13 and 14 are now used for reducing the E_b/N_0 value γ by the stepsize κ. Note that if $(\gamma - \kappa)$ was found to be in the set Γ, this implies that we have already carried out the search based on this particular $(\gamma - \kappa)$ value before. In this case, the stepsize κ will be halved, as shown in Block 13, before the current γ value is reduced by κ dB. The appropriate counterpart operations are carried out in Blocks 7, 8 and 9, where the E_b/N_0 value γ is increased by the stepsize κ, when no polynomial was found in the set $\mathcal{G}$. Again, the step size will be halved, if necessary in order to avoid repeating the same search. When there are only upto 10 elements in the set $\mathcal{G}$, we will store them at Block 15. The union bounds of the TTCM schemes employing these top 10 g_r polynomials will be computed. Note that the best code selected exhibits the best decoding convergence, but not necessarily the lowest error floor among the top 10 polynomials. Hence, if the error floor of the best code is too high, one may consider the other 9 candidates, which may provide a lower error floor at the cost of a slightly worse decoding convergence.

Let us now consider the operational steps, when searching for the constituent TCM code GPs for the 16-state 32QAM-based IQ-TTCM scheme. More specifically, the associated channel capacity is given by $\omega = 9.98$ dB [6, p. 751]. Hence, according to the fourth initialisation parameter, the TCM scheme's parity GP search commences at $\gamma = \omega + 0.5 = 10.48$ dB. It takes three consecutive $\kappa = 0.2$ dB steps in the negative direction, one $\kappa = 0.1$ dB step in the positive direction and another $\kappa = 0.05$ dB in the positive direction, as shown below:

$$10.48\text{dB} \overset{\kappa=-0.2}{\Longrightarrow} 10.28\text{dB} \overset{\kappa=-0.2}{\Longrightarrow} 10.08\text{dB}$$
$$\overset{\kappa=-0.2}{\Longrightarrow} 9.88\text{dB} \overset{\kappa=0.1}{\Longrightarrow} 9.98\text{dB} \overset{\kappa=0.05}{\Longrightarrow} 10.03\text{dB}$$

before finding the best TCM parity bit polynomial, where the estimated minimum SNR required for achieving decoding convergence is $E_b/N_0 = 10.03$ dB. Hence, the constituent TCM

code search designed for constructing capacity-approaching TTCM schemes consists of a number of consecutive EXIT chart evaluations and a search in a one-dimensional continuous space along the E_b/N_0 axis.

Note that, a TTCM scheme could also employ two non-identical constituent TCM component codes. In that case, the code search algorithm depicted in Fig. 4 may be employed for matching the EXIT chart curve of one constituent TCM code to that of the other. However, in this paper we only consider classic TTCM schemes employing two identical constituent TCM codes.

VI. Results and Discussions

Modulation/ States	Polynomial (Octal) $[g_r\ g_1\ g_2\ g_3 \ldots]$	Thresholds (dB) Est.	Thresholds (dB) Actual	ω (dB)	m (bit)
8PSK/4	[7 2 4]	5.75	6.50	5.38	2
8PSK/8	[13 2 4] *	5.17	5.47		
16QAM/8	[11 2 4 10]	8.41	8.20	7.57	3
16QAM/16	[27 2 4 10]	8.17	8.17		
32QAM/16	[37 2 4 10 20] *	10.03	10.20	9.98	4
32QAM/32	[41 2 4 10 20] *	9.90	10.20		
64QAM/32	[41 2 4 10 20 40]	13.40	13.30	12.71	5
64QAM/64	[103 2 4 10 20 40]	13.43	13.48		

TABLE I

IQ-TTCM GPs for uncorrelated Rayleigh fading channels. The codes using GPs marked with * yield a performance less than 0.5 dB away from the channel capacity.

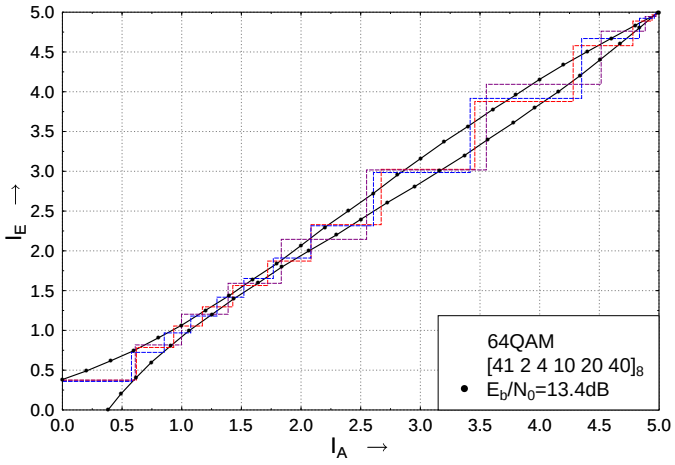

Fig. 5. EXIT chart for the 64QAM-based IQ-TTCM scheme and three snapshot decoding trajectories recorded for the transmission over uncorrelated Rayleigh fading channels using a block-length of $50,000$ symbols, 32-state rate-$5/6$ TCM codes.

We assume that perfect channel state information is available at the receiver. The TCM constituent codes found by the code search algorithm for IQ-TTCM schemes designed for communicating over uncorrelated Rayleigh fading channels are tabulated in Tab. I for 8PSK, 16QAM, 32QAM and 64QAM signal sets. The EXIT chart based estimation and the simulation based E_b/N_0 threshold values marking the edge of the BER curve's waterfall region were tabulated and compared to the channel capacity limits ω in the table. The simulation-based threshold corresponds to those E_b/N_0-values, for which a BER $\approx 10^{-4}$ is achieved using a block length of $100,000$ symbols. The EXIT charts and the corresponding decoding trajectories of the 64QAM-based IQ-TTCM scheme are shown in Fig 5, when communicating over uncorrelated Rayleigh fading channels. As mentioned in Section IV, the EXIT charts were generated based on the assumption that the *extrinsic* information and the systematic information are independent of each other, which has a limited validity. Hence, there are some mismatches between the EXIT charts and the simulation-based decoding trajectories. However, it was found that most of the codes designed perform within 1.0 dB of the channel capacity. This demonstrates the efficiency of the EXIT chart based code-search algorithm proposed in Section V-A.

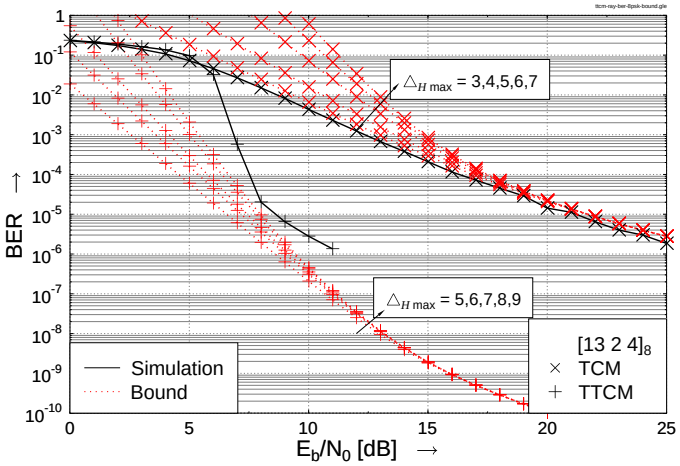

Fig. 6. The BER and union bound performance of the 8PSK-based TCM and TTCM schemes when communicating over uncorrelated Rayleigh fading channels using a block length of $N = 1000$ symbols. The product distance spectrum used for generating the union bound was truncated at $\Delta_{P\,\max} = 60$.

Let us now compare the union bound and the actual BER performance of the various TCM and TTCM schemes. We found that when the product distance Δ_P is sufficiently large, the union bound will only change marginally when higher product distances are considered. Hence, we can truncate the computation of the union bound at a certain maximum product distance $\Delta_{P\,\max}$ in order to minimise the computation time imposed. We found that using $\Delta_{P\,\max} = 60$ is sufficient for the 64QAM based TTCM schemes. Hence, we considered $\Delta_{P\,\max} = 60$ for all schemes for the sake of simplicity, although the required $\Delta_{P\,\max}$ value for lower-order modulation schemes is lower than 60. Fig. 6 shows the effect of truncating the union bounds using different values of maximum Hamming distance $\Delta_{H\,\max}$ at a fixed maximum product distance of $\Delta_{P\,\max} = 60$. As seen in Fig. 6, we need only a low value of $\Delta_{H\,\max} = 4$ and $\Delta_{H\,\max} = 6$ in order to estimate the error floor of TCM and TTCM schemes, respectively. Note that the truncated union bound matches well with the BER of the TCM schemes, but there is a gap between the truncated union bound and the BER of the TTCM schemes. We note from [19, Fig. 8] that there is also a gap between the truncated union bound and the BER of binary turbo codes. This gap is mainly due to the employment of the uniform interleaver concept in the computation of the union bound, where the performance of the turbo codes or

TTCM is averaged over all possible interleavers. Furthermore, employing only the all-zero encoded symbol sequence in the computation of the TTCM union bound may also contribute to this gap, if the employed constituent TCM scheme is not strong-sense regular. We consider all possible encoded symbol sequences in the Monte Carlo simulations.

We fixed $\Delta_{P\max} = 60$ and computed a truncated union bound using $\Delta_{H\max} = 4$ and $\Delta_{H\max} = 6$ for the TCM and TTCM schemes, respectively. The number of turbo iterations for the TTCM schemes was fixed to 16. As we can see from Figs. 7, 8 and 9, the estimated union bounds of the 8PSK, 16QAM and 32QAM based TCM schemes exhibit a good match with respect to the corresponding BER curves. As shown in Figs. 7 to 10, the estimated union bounds for the TTCM schemes are lower than the actual TTCM BER curves. However, the TTCM union bounds seemed to have a good match to the IQ-TTCM BER curves in the context of the 8PSK, 16QAM, 32QAM and 64QAM modulation schemes considered. Hence, we can apply the TTCM union bound to generate a good measure of the expected IQ-TTCM error floor.

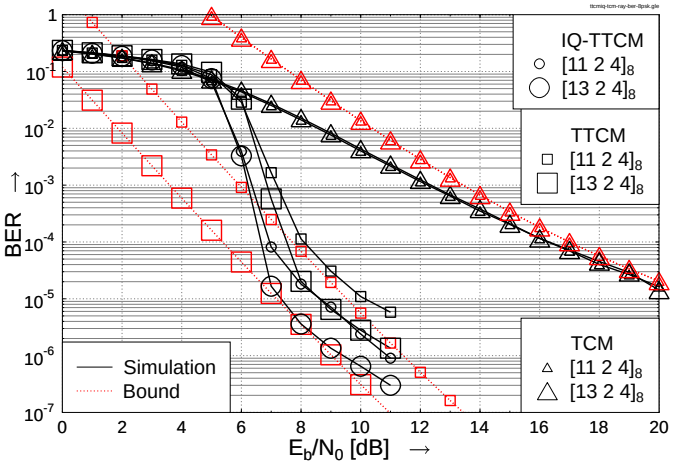

Fig. 7. The BER and union bound performance of the 8PSK-based TCM and (IQ-)TTCM schemes when communicating over uncorrelated Rayleigh fading channels using a block length of $N = 1000$ symbols. The product distance spectrum used for generating the union bound was truncated at $\Delta_{P\max} = 60$.

As seen from Fig. 7, the BER performance of the 8PSK based TCM schemes employing the GPs of $[11\ 2\ 4]_8$ and $[13\ 2\ 4]_8$ is very similar. Likewise, observe in Fig. 8 that the GPs $[21\ 2\ 4\ 10]_8$ and $[17\ 2\ 4\ 10]_8$ result in a similar BER for the 16QAM based TCM schemes. This is because their distance spectra are similar. However, as seen in Eq. (16), the WEF of TTCM is the product of the WEFs of its constituent TCM codes. The product distance and Hamming distance of TTCM as given by Eq. (6) and Eq. (7), respectively, are also different from that of its constituent TCM codes. Hence the marginal difference in terms of the TCM distance spectrum is further emphasized when using two different GPs. Therefore, the BER performance curves of the resultant (IQ-)TTCM schemes are significantly different, when employing two different GPs, as seen in Figs. 7 and 8. More explicitly, the 8PSK (IQ-)TTCM scheme performs one dB better, when employing the proposed GP of $[13\ 2\ 4]_8$ compared to the GP of $[11\ 2\ 4]_8$ adopted from [4]. We found that the octally

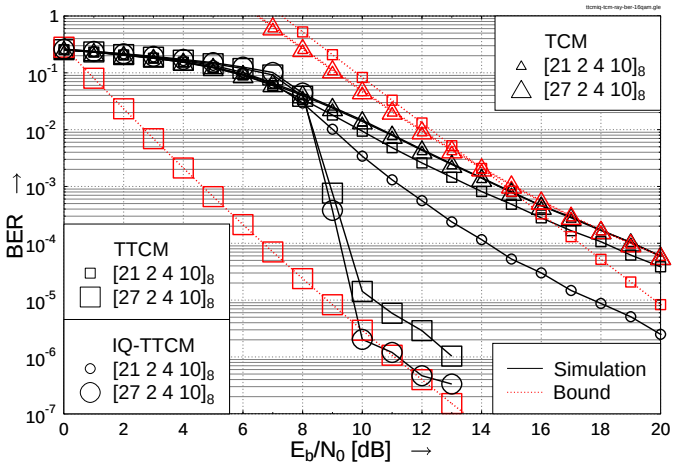

Fig. 8. The BER and union bound performance of the 16QAM-based TCM and (IQ-)TTCM schemes when communicating over uncorrelated Rayleigh fading channels using a block length of $N = 1000$ symbols. The product distance spectrum used for generating the union bound was truncated at $\Delta_{P\max} = 60$.

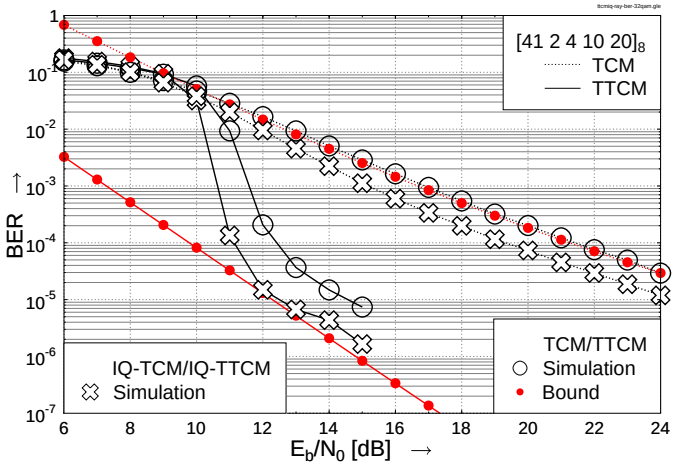

Fig. 9. The BER and union bound performance of the 32QAM-based (IQ-)TCM and (IQ-)TTCM schemes when communicating over uncorrelated Rayleigh fading channels using a block length of $N = 1000$ symbols. The product distance spectrum used for generating the union bound was truncated at $\Delta_{P\max} = 60$.

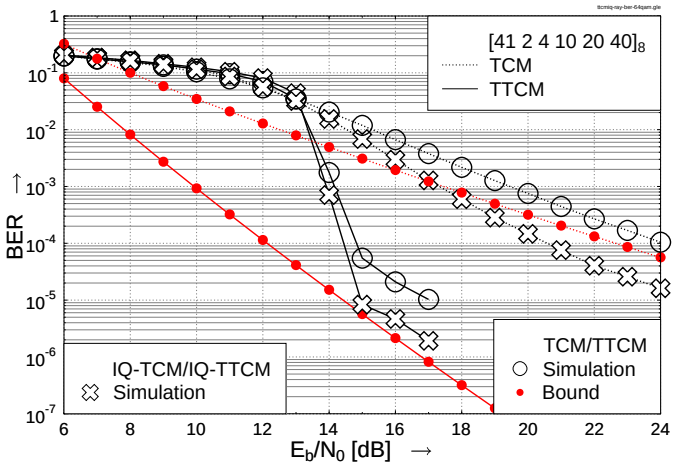

Fig. 10. The BER and union bound performance of the 64QAM-based (IQ-)TCM and (IQ-)TTCM schemes when communicating over uncorrelated Rayleigh fading channels using a block length of $N = 1000$ symbols. The product distance spectrum used for generating the union bound was truncated at $\Delta_{P\max} = 60$.

represented GP $[21\ 2\ 4\ 10]_8$, which was designed for a 16QAM TTCM scheme based on the 'punctured' minimal distance criterion of [4] was unable to achieve full decoding convergence due to having a closed tunnel in its EXIT chart. Hence, the BER performance of the 16QAM TTCM scheme employing the proposed GP of $[27\ 2\ 4\ 10]_8$ is significantly better than that of the benchmarkers, as it is evidenced in Fig 8.

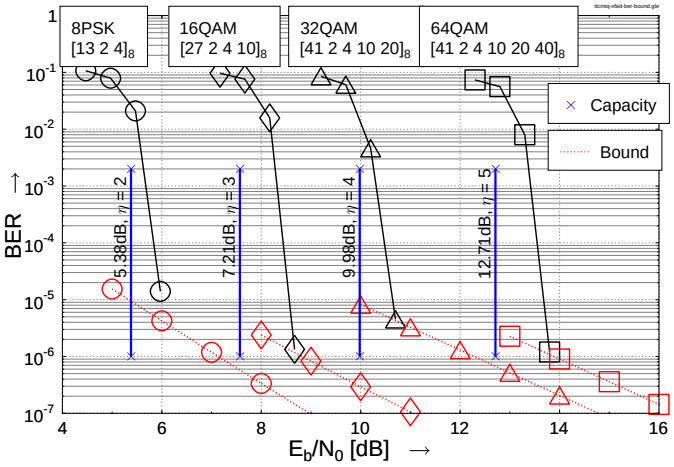

Fig. 11. The BER and the error floor bound performance of the various IQ-TTCM schemes when communicating over uncorrelated Rayleigh fading channels using a block length of $N = 10,000$ symbols. The product distance spectrum and Hamming distance spectrum used for generating the union bound was truncated at $\Delta_{P\,\max} = 60$ and $\Delta_{H\,\max} = 6$, respectively.

As depicted in Fig. 11, when we increased the block length to $N = 10,000$ symbols, the IQ-TTCM schemes exhibit lower error floors and a decoding convergence closer to the estimated thresholds summarised in Tab. I, compared to the scenario using a block length of $N = 1000$ symbols, as shown in Figs. 7 to 10. Hence, capacity-approaching TTCM schemes can be successfully designed based on the proposed symbol-based EXIT chart aided and the truncated union bound assisted code design. Furthermore, the proposed technique may also be employed for designing symbol-interleaved space-time TTCM schemes for approaching the multiple-input multiple-output channel capacity.

VII. Conclusions

We have designed capacity-approaching TTCM schemes by performing a search for good constituent TCM component codes with the aid of symbol-based EXIT charts and truncated symbol-based union bounds. The prime design criterion of capacity-approaching TTCM schemes is that of finding an open tunnel in the corresponding EXIT charts at the lowest possible SNR values, while maintaining a sufficiently low error floor, rather than maximising the 'punctured' minimal distance of the constituent codes [4]. Hence, we can reduce the code search space by fixing the feed-forward GPs and then search for the best feed-back GP that provides an open tunnel in the EXIT chart at the lowest possible SNR value. Although the independence of the *extrinsic* information and systematic information is not always satisfied by the symbol-based TTCM scheme, most of the good constituent codes found assist the TTCM schemes in performing near the channel capacity.

Appendix

The set $\chi = \chi(y, m) = \{z\}$ in Eq. (19) can be generated by using the following recursive function:
Find_Symbol_Error_Set(y, m, χ, 0), which is defined as:
Find_Symbol_Error_Set(*int* $\tilde{y}$, *int* b, *int** χ, *int* $\bar{z}$)*{*

if $(b = 1)$ *add* $(\bar{z} + \tilde{y})$ *into* χ
else {
for $(z_b = 0; z_b \leq \left\lfloor \frac{\tilde{y}}{b} \right\rfloor; z_b + +)$
Find_Symbol_Error_Set$(\tilde{y} - b \cdot z_b, b - 1, \chi, \bar{z} + z_b)$
}
return
}

where the values of the variables $\tilde{y}$, b and $\bar{z}$ could change during the transition from the parent loop to the child loops.

References

[1] G. Ungerböck, "Channel coding with multilevel/phase signals," *IEEE Transactions on Information Theory*, vol. 28, pp. 55–67, January 1982.
[2] D. Divsalar and M. K. Simon, "The design of trellis coded MPSK for fading channel: Performance criteria," *IEEE Transactions on Communications*, vol. 36, pp. 1004–1012, September 1988.
[3] D. Divsalar and M. K. Simon, "The design of trellis coded MPSK for fading channel: Set partitioning for optimum code design," *IEEE Transactions on Communications*, vol. 36, pp. 1013–1021, September 1988.
[4] P. Robertson, T. Wörz, "Bandwidth-efficient turbo trellis-coded modulation using punctured component codes," *IEEE Journal on Selected Areas in Communications*, vol. 16, pp. 206–218, February 1998.
[5] C. Berrou, A. Glavieux and P. Thitimajshima, "Near shannon limit error-correcting coding and decoding : Turbo codes," in *Proceedings, IEEE International Conference on Communications*, pp. 1064–1070, 1993.
[6] L. Hanzo, S. X. Ng, W. Webb and T. Keller, *Quadrature Amplitude Modulation: From Basics to Adaptive Trellis-Coded, Turbo-Equalised and Space-Time Coded OFDM, CDMA and MC-CDMA Systems, Second Edition*. New York, USA : John Wiley and Sons, 2004.
[7] S. X. Ng, T. H. Liew, L-L. Yang and L. Hanzo, "Comparative study of TCM, TTCM, BICM and BICM-ID schemes," in *IEEE Vehicular Technology Conference*, (Rhodes, Greece), pp. 2450–2454, May 2001.
[8] E. Zehavi, "8-PSK trellis codes for a Rayleigh fading channel," *IEEE Transactions on Communications*, vol. 40, pp. 873–883, May 1992.
[9] S. Le Goff, A. Glavieux and C. Berrou, "Turbo-codes and high spectral efficiency modulation," in *Proceedings of IEEE International Conference on Communications*, pp. 645–649, 1994.
[10] T. Duman and M. Salehi, "The union bound for turbo-coded modulation systems over fading channels," *IEEE Transactions on Communications*, vol. 47, pp. 1495–1502, October 1999.
[11] C. Fragouli and R. D. Wesel, "Turbo-encoder design for symbol-interleaved parallel concatenated trellis-coded modulation," *IEEE Transactions on Communications*, vol. 49, pp. 425–435, March 2001.
[12] B. Scanavino, G. Montorsi, and S. Benedetto, "Convergence properties of iterative decoders working at bit and symbol level," in *IEEE Globecom*, (San Antonio, TX), pp. 1037–1041, November 2001.
[13] J. Boutros and E. Viterbo, "A power- and bandwidth-efficient diversity technique for the Rayleigh fading channel," *IEEE Transactions on Information Theory*, vol. 44, pp. 1453–1467, July 1998.
[14] B. D. Jelicic and S. Roy, "Design of trellis coded QAM for flat fading and AWGN channels," *IEEE Transactions on Vehicular Technology*, vol. 44, pp. 192–201, February 1994.
[15] S. X. Ng and L. Hanzo, "Space-time IQ-interleaved TCM and TTCM for AWGN and Rayleigh fading channels," *IEE Electronics Letters*, vol. 38, pp. 1553–1555, November 2002.
[16] J. Yuan, B. Vucetic and W. Feng, "Combined turbo codes and interleaver design," *IEEE Transactions on Communications*, vol. 47, pp. 484–487, April 1999.

[17] W. Feng, J. Yuan and B. Vucetic, "A code-matched interleaver design for turbo codes," *IEEE Transactions on Communications*, vol. 50, pp. 926–937, June 2002.
[18] S. X. Ng, T. H. Liew, L-L. Yang and L. Hanzo, "Binary BCH turbo coding performance: Union bound and simulation results," in *IEEE Vehicular Technology Conference*, (Tokyo, Japan), pp. 849–853, May 2000.
[19] Lance C. Perez, Jan Seghers and Daniel J. Costello, "A distance spectrum interpretation of turbo codes," *IEEE Transactions on Information Theory*, vol. 42, pp. 1698–1709, November 1996.
[20] D. Tujkovic, "Unified approach to single- and multiantenna turbo-TCM: union bound and constituent code optimization over AWGN and fading channels," *in Proceedings of 2004 International Symposium on Personal, Indoor and Mobile Radio Communications*, vol. 3, pp. 1618–1622, September 2004.
[21] S. ten Brink, "Convergence behaviour of iteratively decoded parallel concatenated codes," *IEEE Transactions on Communications*, vol. 49, pp. 1727–1737, October 2001.
[22] A. Grant, "Convergence of non-binary iterative decoding," in *Proceedings of the IEEE Global Telecommunications Conference (GLOBECOM)*, (San Antonio TX, USA), pp. 1058–1062, November 2001.
[23] J. Kliewer, S. X. Ng, and L. Hanzo, "Efficient computation of EXIT functions for non-binary iterative decoding," *IEEE Transactions on Communications*, vol. 54, pp. 2133–2136, December 2006.
[24] S. ten Brink, "Rate one-half code for approaching the Shannon limit by 0.1 dB," *IEE Electronics Letters*, vol. 36, pp. 1293–1294, July 2000.
[25] M. Tüchler and J. Hagenauer, "EXIT charts and irregular codes," in *Proceeding of the 36th Annual Conference on Information and System Sciences*, (Princeton, NJ, USA), March 2002.
[26] S. Siwamogsatham, M. P. Fitz and J. H. Grimm, "A new view of performance analysis of transmit diversity schemes in correlated rayleigh fading," *IEEE Transactions on Information Theory*, vol. 48, pp. 950–956, April 2002.
[27] C. Schlegel, "Chapter 5: Performance bounds," in *Trellis Coding*, (New York), pp. 121–151, September 1997.
[28] S. Lin and D. J. Costello, Jr, *Error Control Coding: Fundamentals and Applications*. Inc. Englewood Cliffs, New Jersey 07632: Prentice-Hall, 1983.
[29] S. Benedetto, M. Mondin and G. Montorsi, "Performance evaluation of trellis-coded modulation schemes," *Proceedings of the IEEE*, vol. 82, pp. 833–855, June 1994.
[30] Sergio Benedetto and Guido Montorsi, "Unveiling turbo codes: Some results on parallel concatenated coding schemes," *IEEE Transactions on Information Theory*, vol. 42, pp. 409–428, March 1996.
[31] H. Chen and A. Haimovich, "EXIT charts for turbo trellis-coded modulation," *IEEE Communications Letters*, vol. 8, pp. 668–670, November 2004.

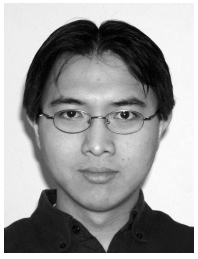

Soon Xin Ng (S'99–M'03) received the B.Eng. degree (First class) in electronics engineering and the Ph.D. degree in wireless communications from the University of Southampton, Southampton, U.K., in 1999 and 2002, respectively. From 2003 to 2006, he was a postdoctoral research fellow at the University of Southampton working on collaborative European research projects known as SCOUT, NEWCOM and PHOENIX. Since August 2006, he has been a lecturer in wireless communications at the University of Southampton. His research interests include adaptive coded modulation, channel coding, space-time coding, joint source and channel coding, OFDM and MIMO. He has published numerous papers and coauthored a book in this field.

Osamah Rashed Alamri (S'02) received his B.Sc. degree with first class honours in electrical engineering from King Fahd University of Petroleum and Minerals (KFUPM), Dhahran, Saudi Arabia, in 1997, where he was ranked first. In 2002, he received his M.Sc. degree in electrical engineering from Stanford University, California, USA. He received his Ph.D. degree in wireless communications from the University of Southampton, Southampton, U.K., in 2007 and he is currently a visiting scholar at the same institution. His research interests include sphere packing modulation, space-time coding, turbo coding and detection, adaptive receivers and MIMO systems.

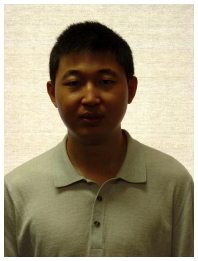

Yonghui Li (M'04) received his PhD degree in Electronic Engineering in November 2002 from Beijing University of Aeronautics and Astronautics. From 1999–2003, he was affiliated with Linkair Communication Inc, where he held a position of project manager with responsibility for the design of physical layer solutions for LAS-CDMA system. Since 2003, he has been with Telecommunication Lab, University of Sydney, Australia. He is now a lecturer in School of Electrical and Information Engineering, University of Sydney. He was awarded Australian Queen Elizabeth II fellowship in 2008.

His current research interests are in the area of wireless communications, with a particular focus on MIMO, cooperative communications, coding techniques and wireless sensor networks. He holds a number of patents granted and pending in these fields. He is an Associate Editor for EURASIP Journal on Wireless Communications and Networking, and Editor for Journal of Networks. He also served as Editor for special issue on "advances in error control coding techniques" in EURASIP Journal on Wireless Communications and Networking, He has also been involved in the technical committee of several international conferences, such as ICC, PIMRC, WirelessCom and so on.

Jörg Kliewer (S'97–M'99–SM'04) received the Dipl.- Ing. (M.Sc.) degree in Electrical Engineering from Hamburg University of Technology, Hamburg, Germany, in 1993, and the Dr.-Ing. degree (Ph.D.) in Electrical Engineering from the University of Kiel, Kiel, Germany, in 1999, respectively. From 1993 to 1998, he was a Research Assistant at the University of Kiel, and from 1999 to 2004, he was a Senior Researcher and Lecturer with the same institution. In 2004 he visited the University of Southampton, U.K., for one year, and from 2005 to 2007 he was with the University of Notre Dame, Notre Dame, IN, as a Visiting Assistant Professor. In August 2007 he joined New Mexico State University, Las Cruces, NM, as an Assistant Professor. His research interests include joint source-channel coding, error-correcting codes, wireless communications, and communication networks. Dr. Kliewer was the recipient of a Leverhulme Trust Award and a German Research Foundation Fellowship Award in 2003 and 2004, respectively. He is a member of the Editorial Board of the EURASIP Journal on Advances in Signal Processing.

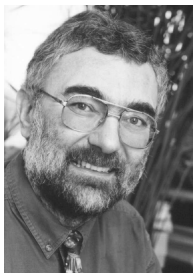

Lajos Hanzo (M'91–SM'92–F'04) Fellow of the Royal Academy of Engineering, received his first-class degree in electronics in 1976 and his doctorate in 1983. In 2004 he was awarded the Doctor of Sciences (DSc) degree by the University of Southampton, UK. During his career in telecommunications he has held various research and academic posts in Hungary, Germany and the UK. Since 1986 he has been with the Department of Electronics and Computer Science, University of Southampton, UK, where he holds the chair in telecommunications. He has co-authored 12 books, totalling 9000 pages on mobile radio communications, published in excess of 600 research papers, has acted as TPC Chair of numerous major IEE and IEEE conferences, presented various keynote lectures and has been awarded a number of distinctions. Currently he heads an academic research team, working on a range of research projects in the field of wireless multimedia communications sponsored by industry, the Engineering and Physical Sciences Research Council (EPSRC) UK, the European IST Programme and the Mobile Virtual Centre of Excellence (VCE), UK. He is an enthusiastic supporter of industrial and academic liaison and he offers a range of industrial courses. Lajos is also an IEEE Distinguished Lecturer of both the Communications as well as the Vehicular Technology Society, a Fellow of both the IEEE and the IEE. He is an editorial board member of the Proceedings of the IEEE and a Governer of the IEEE VT Society. For further information on research in progress and associated publications, please refer to http://www-mobile.ecs.soton.ac.uk